Novel derivatives of 1, 3, 4-oxadiazoles are potent mitostatic agents featuring strong microtubule depolymerizing activity in the sea urchin embryo and cell culture ...

14 AUTHORS, INCLUDING:

Heiko Lemcke
University of Rostock
11 PUBLICATIONS 97 CITATIONS

SEE PROFILE

Dieter G. Weiss
Institut für Zelltechnologie IZT e.V.
152 PUBLICATIONS 3,315 CITATIONS

SEE PROFILE

Victor V Semenov
N. D. Zelinsky Institute of Organic Chemistry
234 PUBLICATIONS 1,011 CITATIONS

SEE PROFILE

Original article

Novel derivatives of 1,3,4-oxadiazoles are potent mitostatic agents featuring strong microtubule depolymerizing activity in the sea urchin embryo and cell culture assays

Alex S. Kiselyov [a,*], Marina N. Semenova [b], Natalya B. Chernyshova [c], Andrei Leitao [d], Alexandr V. Samet [c], Konstantine A. Kislyi [c], Mikhail M. Raihstat [c], Tudor Oprea [d], Heiko Lemcke [e], Margaréta Lantow [e], Dieter G. Weiss [e], Nazli N. Ikizalp [f], Sergei A. Kuznetsov [e], Victor V. Semenov [c,f]

[a] deCODE Chemistry, 2501 Davey Road, Woodridge, Chicago, IL 60616, USA
[b] Institute of Developmental Biology, RAS 26 Vavilov Str., Moscow 119334, Russia
[c] Zelinsky Institute of Organic Chemistry, RAS 47 Leninsky Prospect, Moscow 117913, Russia
[d] Department of Biocomputing, University of New Mexico, Albuquerque, NM, USA
[e] Institute of Biological Sciences University of Rostock, 3 Albert-Einstein-Str., D-18059 Rostock, Germany
[f] Chemical Block Ltd., 3 Kyriacou Matsi, Limassol 3723, Cyprus

ARTICLE INFO

ABSTRACT

A series of novel 1,3,4-oxadiazole derivatives based on structural and electronic overlap with combretastatins have been designed and synthesized. Initially, we tested all new compounds in vivo using the phenotypic sea urchin embryo assay to yield a number of agents with anti-proliferative, anti-mitotic, and microtubule destabilizing activities. The experimental data led to identification of 1,3,4-oxadiazole derivatives with isothiazole (5–8) and phenyl (9–12) pharmacophores featuring activity profiles comparable to that of combretastatins, podophyllotoxin and nocodazole. Cytotoxic effects of the two lead molecules, namely 6 and 12, were further confirmed and evaluated by conventional assays with the A549 human cancer cell line including cell proliferation, cell cycle arrest at the G2/M phase, cellular microtubule distribution, and finally in vitro microtubule assembly with purified tubulin. The modeling results using 3D similarity (ROCS) and docking (FRED) correlated well with the observed activity of the molecules. Docking data suggested that the most potent molecules are likely to target the colchicine binding site.

© 2010 Elsevier Masson SAS. All rights reserved.

1. Introduction

Targeting tubulin in rapidly dividing tumor cells has been a well-validated strategy for cancer therapy [1–3]. Screening of natural products for cytotoxic activity yielded numerous structurally diverse classes of mitotic spindle poisons [4–7]. Current evidence suggests that these natural products affect tubulin polymerization dynamics by binding to microtubules (MT) at discrete regions [8], such as well-characterized taxoid, vinca alkaloid and colchicine sites [9–11]. Paclitaxel (Taxol®) and Vinblastine binding to the former two sites have been successfully used in clinics as chemotherapeutics to treat various tumor types. However, high toxicity, non-linear pharmacology together with the development of drug resistance found for

these mitotic poisons [12–16] prompted scientists to expand search for synthetic modulators of tubulin that a) bind to alternative site(s) [17]; b) mimic natural products, are synthetically feasible and drug-like, c) result in the same anti-mitotic effect, and d) display better therapeutic window. Many natural and synthetic compounds with different molecular structure have been identified as colchicine site ligands [7,18–20]. Podophyllotoxin (Scheme 1) is another example of the natural product that binds to the colchicine (or adjacent) site on tubulin [11,20]. These colchicine site binders share "homology" with the A and C rings of colchicine described as a tilted "biaryl" system connected by a hydrocarbon bridge of variable length (ex., B and E rings of podophyllotoxin, Scheme 1), although different binding modes for the two molecules have been introduced (reviewed in [20]).

Synthetic derivatives of combretastatins, CA-4 phosphate, AVE8062, and ZD-6126 are in clinical trials as potent antineoplastic agents [3,18,20].

* Corresponding author. Tel.: +1 630 783 4951.
E-mail address: akiselyov@decode.com (A.S. Kiselyov).
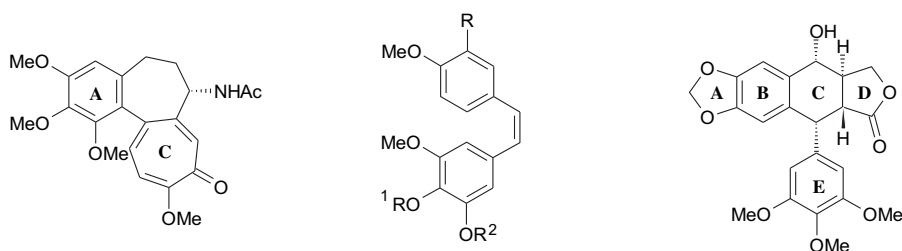
Scheme 1. Colchicine R = OH, R^1 = R^2 = Me, Combretastatin A-4 (CA-4) Podophyllotoxin R = OH,R^1, R^2 = –CH_2–, Combretastatin A-2 (CA-2)R = OPO_3Na_2, R^1 = R^2 = Me, CA4-P.

2. Results and discussion

In our search for the synthetic anti-mitotic agents binding to tubulin, we selected the 1,3,4-oxadiazole template as a starting point [21]. Earlier analogs from these series featured good potency in the _in vitro_ tubilin polymerization assay, caused mitotic arrest in cells derived from multi-drug resistant tumors. In this paper, we report on the development of a robust and high-yielding synthetic procedure to access novel 1,3,4-oxadiazole derivatives **1–25** that specifically affect tubulin dynamics (Table 1). Furthermore, in order to evaluate anti-mitotic activity of these small molecules we introduced reliable phenotypic assay based on the sea urchin embryo [22,23]. This _in vivo_ screening yielded a rapid "one pot" assessment of anti-proliferative,
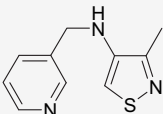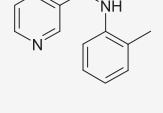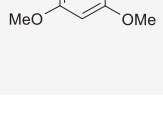
anti-mitotic, and cytotoxic effects of the oxadiazoles **1–25** on a living organism. In addition, the assay allowed for the expeditious ranking of the molecules based on their relative activity. The sea urchin embryo model conveniently differentiates tubulin-independent anti-proliferative activity and cytotoxicity/embryotoxicity of tested compounds. During cleavage stages, intensive synchronous cell divisions are observed, whereas processes of differentiation and morphogenesis become dominant from gastrulation. Tubulin-independent anti-proliferative/anti-mitotic agents cause cleavage alteration along with the inability to affect the embryo development after hatching at the same concentration range. In contrast, toxicity implies embryo abnormalities observed after treatment of both fertilized eggs and hatched blastulae. The intrinsic mechanisms of action of tubulin-

Table 1
Structure Activity Relationship Studies of 1,3,4-Oxadiazoles **1–25** in the Sea Urchin Embryo Assay.
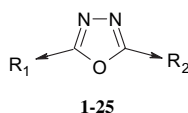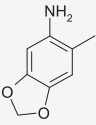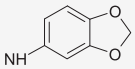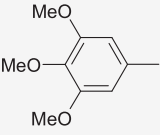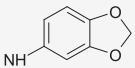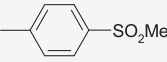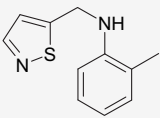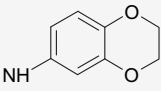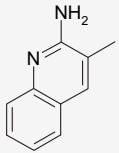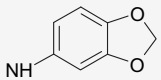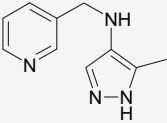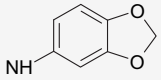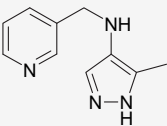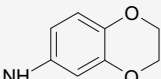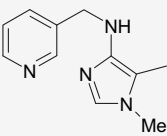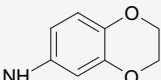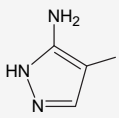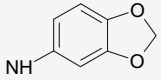
Cmpd ID	R_1	R_2	EC$_{50}$, µM[a]		
			Cleavage Alteration	Cleavage Arrest	Spinning
CA-2			0.002	0.01	0.05
CA-4P			0.005	0.01	1
Podophyllotoxin			0.02	0.05	0.5
Nocodazole			0.005	0.01	0.1
1			0.5[b]	4	>5
2			NT	NT	NT
3			0.2	0.5	0.5
4			0.5	2	>2.5

Table 1 (*continued*)

Cmpd ID	R₁	R₂	EC₅₀, µM[a]		
			Cleavage Alteration	Cleavage Arrest	Spinning
5			0.002	0.005	0.02
6			0.002	0.005	0.1
7			0.005	0.05	0.05
8			0.005	0.01	0.1
9			0.001	0.005	0.005
10			0.001	0.005	0.005
11			0.0005	0.002	0.005
12			0.0005	0.002	0.005
13			0.001	0.01	1
14			0.001	0.02	0.1
15			0.025	0.1	0.2
16			0.05	0.2	1

Table 1 (*continued*)

Cmpd ID	R₁	R₂	EC₅₀, μM[a]		
			Cleavage Alteration	Cleavage Arrest	Spinning
17			0.05	0.5	0.2
18			0.4[b,c]	1	>5
19			4[b]	>4	>5
20			2	5	5
21			0.05	2	>2
22			1[b]	>10	>10
23			1[b]	>10	>10
24			0.2[b]	1	>2.5
25			>20	>20	>20

[a] The sea urchin embryo assay was conducted as described in [22], duplicate measurements showed no differences in threshold concentration values.
[b] Anti-proliferative activity that is non-tubulin related.
[c] Molecule displayed post-hatching embryo toxicity at ≥1 μM when applied after hatching (see discussion below). NT – not tested.

independent anti-proliferative/anti-mitotic compounds can be further elucidated in detail using the appropriate screening systems [22]. Cytotoxic properties of selected compounds were further evaluated by conventional cell-based assays with human cancer cells, and by inhibition of purified tubulin polymerization *in vitro*. To rationalize the tubulin activity of 1,3,4-oxadiazole derivatives, we

conducted a series of three-dimensional (3D) similarity comparisons. Our computational insight suggested that the most active 1,3,4-oxadiazoles capture the overall configuration of combretastatins.

2.1. Chemical synthesis of 1,3,4-oxadiazoles

We used two related synthetic approaches to access the targeted 1,3,4-oxadiazoles, as shown on Scheme 2. Following route 1, the isothiazole derivative was treated with neat hydrazine hydrate at reflux for 4 h to yield the respective hydrazide in 70% yields. In order to assemble the 1,3,4-oxadiazole ring, the hydrazide was reacted with isothiocyanates Ar^1-NCS followed by in situ cyclization of the intermediate thiosemicarbazides with DCC to afford the key precursor molecules 1–3 in 56–80% isolated yields. Pharmacophore Ar^2 was introduced into the amines 1–3 via the initial formation of the respective Schiff bases followed by their $NaBH_4$-mediated reduction to furnish the targeted compounds 5, 7 and 8 (84–88% yield). Notably, our attempts to accomplish a one-pot reductive amination of 1–3 under a variety of experimental conditions consistently afforded lower yields (by ca. 15–30%) of the final heterocycles. Furthermore, we were unable to synthesize 6 following the procedure described above (Scheme 2, Route 1). In order to address this issue, we devised the alternative route 2 (Scheme 2).

It involved a reversed synthetic sequence starting with the introduction of Ar^2 followed by the installation of the 1,3,4-oxadiazole moiety to yield the targeted compounds 4 and 6 (75–80% yield). Additional test molecules were synthesized using related synthetic sequences involving the formation of the diverse aromatic or heterocyclic ortho-amino hydrazides as described in the Supporting Information.

2.2. Biological activity

2.2.1. Evaluation of 1,3,4-oxadiazoles in the phenotypic sea urchin embryo assay

We have recently introduced a reliable and reproducible phenotypic sea urchin embryo assay that allows for the selection of potent mechanistically sound compounds targeting tubulin [22].

This simple in vivo model facilitates rapid "one pot" assessment of anti-proliferative, anti-mitotic, and cytotoxic effects of small molecules on a living organism. The assay includes i) fertilized egg test for anti-mitotic activity displayed by the embryo's cleavage alteration/arrest, and ii) behavioral monitoring of a free-swimming blastulae treated immediately after hatching (9–12 h after fertilization). Changes to the embryo swimming pattern, i.e. lack of forward movement, settlement to the bottom of the culture vessel and rapid spinning around the animal–vegetal axis suggests a tubulin destabilizing activity caused by a molecule [22]. Notably, this experiment yields data on both anti-proliferative activity of the test molecule as well as on its tubulin polymerization effect (ex., destabilizing vs stabilizing) (Fig. 1). Data generated by the assay for multiple marketed and experimental anti-mitotics correlated well with their in vitro, ex vivo and in vivo potency and efficacy [22,23].

We have evaluated synthetic molecules 1–25 using the sea urchin embryo test system. Stock solutions of compounds were prepared either in 95% EtOH at 5 mM or in DMSO at 5–10 mM concentrations followed by their 10-fold dilution with 95% EtOH. In our hands, this protocol enhanced solubility of the test compounds in salt-containing medium (sea water), as evidenced by microscopic examination of the samples. Further, we found that the maximal tolerated concentrations of DMSO and EtOH in the in vivo assay were 0.05% and 1% respectively. Higher concentrations of either DMSO ($\geq$0.1%) or EtOH (>1%) caused non-specific alteration and retardation of the sea urchin embryo development independent of the treatment stage. The effects of tested molecules were quantified by a threshold concentration resulting in cleavage abnormalities and embryo death before hatching or full mitotic arrest (Table 1). CA-2, CA-4P (OxiGene), podophyllotoxin (Sigma), and nocodazole (Sigma) served as benchmark reference compounds.

As evidenced from Table 1, CA-2, CA-4P, podophyllotoxin, and nocodazole displayed strong effects on the sea urchin embryos. Effective concentrations of the reference compounds resulting in embryo cleavage alteration/arrest were close to the reported IC_{50} values for a panel of human tumor cell lines [20,22,24]. It is worth

1, Ar^1 = 3,4-(OCH_2O)-C_6H_4-
2, Ar^1 = 3,4-(OCH_2CH_2O)-C_6H_4-
3, Ar^1 = 4-Cl-C_6H_4-

Route 1: used to synthesize 5, 7, 8

Route 2: used to synthesize 4, 6

4, Ar^1 = 4-Cl-C_6H_4-; Ar^2 = 3-Py (80%)
5, Ar^1 = 3,4-(OCH_2O)-C_6H_3- ; Ar^2 = 4-Py (84%)
6, Ar^1 = 3,4-(OCH_2CH_2O)-C_6H_3- ; Ar^2 = 4-Py (75%)
7, Ar^1 = 3,4-(OCH_2O)-C_6H_3- ; Ar^2 = 3-Py (88%)
8, Ar^1 = 3,4-(OCH_2CH_2O)-C_6H_3- ; Ar^2 = 3-Py (84%)
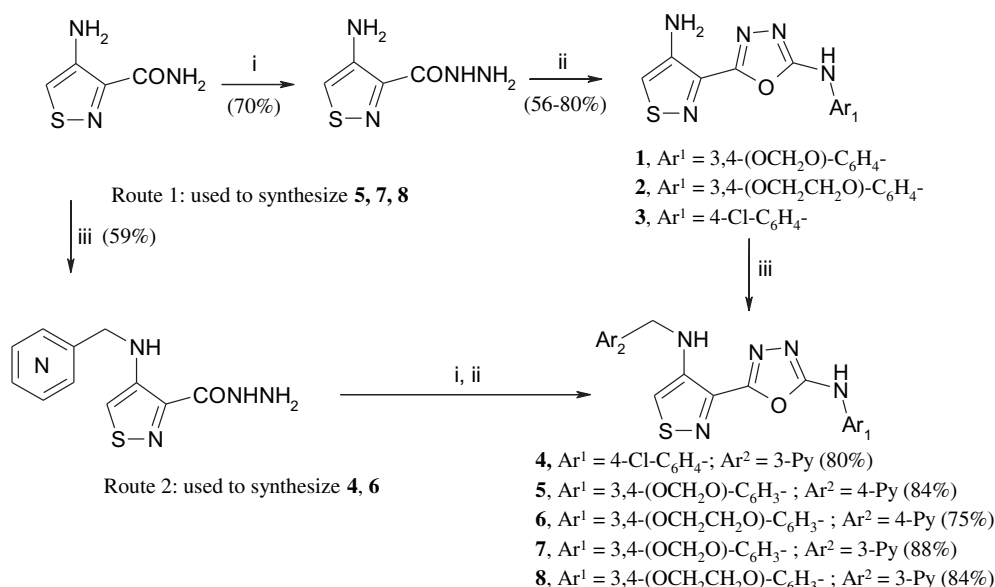
Scheme 2. Reagents and conditions: i) neat $N_2H_4 \cdot H_2O$, reflux, 4 h; ii) R^1–C_6H_4–NCS, tBuOH, reflux 10 min; 50–60 °C, 1h; DCC, MeCN, reflux, 3 h; iii) R^2CHO (R = 3-Py or 4-Py),MeCN, pTsOH, reflux, 3 h; $NaBH_4$, iPrOH, reflux, 3h.

A.S. Kiselyov et al. / European Journal of Medicinal Chemistry 45 (2010) 1683–1697
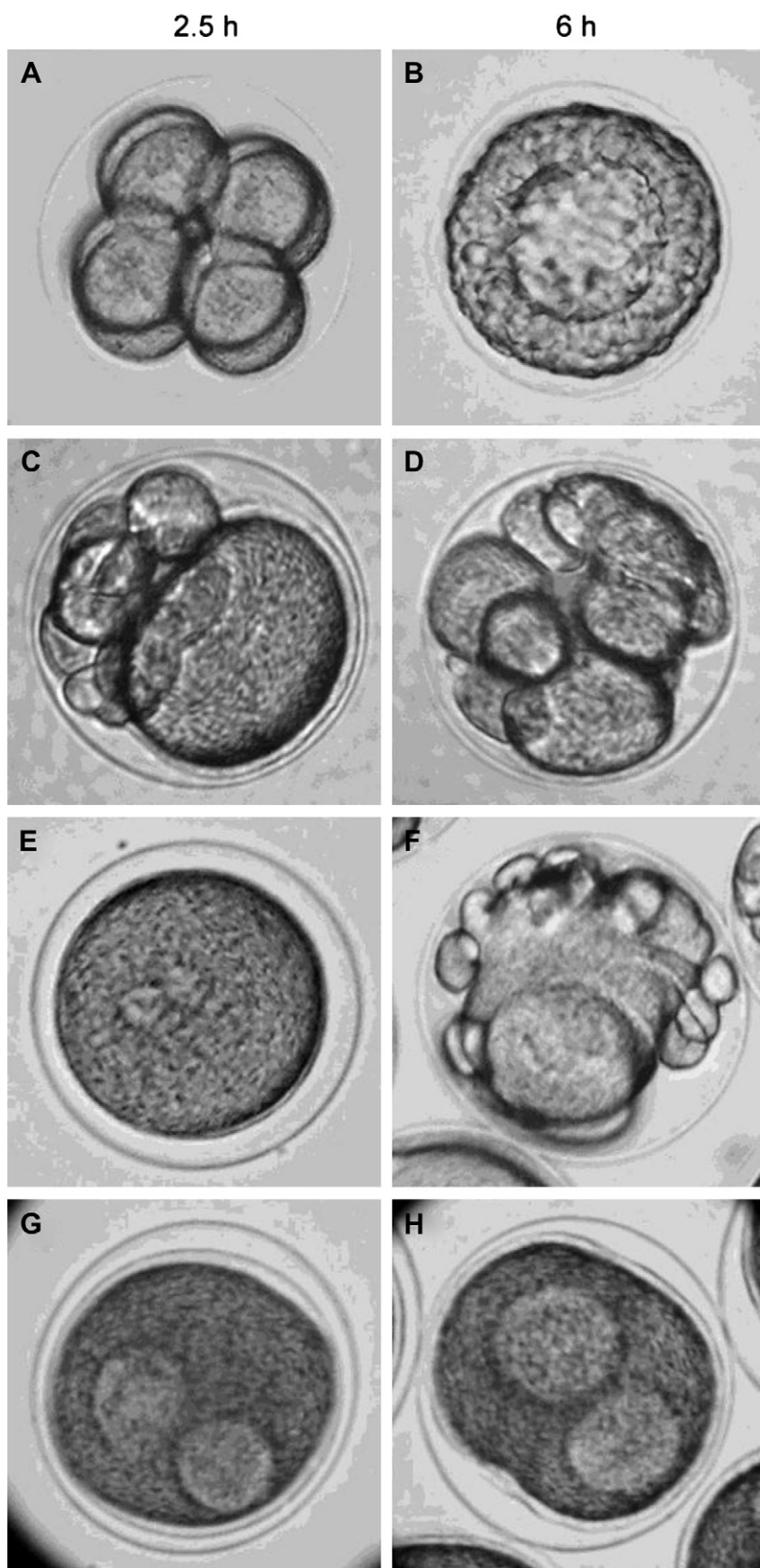
Fig. 1. Typical effects of tubulin-modulating compounds on early sea urchin embryo development. (A, B) Intact embryos. (A) 8-cell stage. (B) Early blastula. Fertilized eggs (10–15 min after fertilization) were exposed continuously to compound 5 at a threshold concentration for cleavage alteration (2 nM; C, D); to compound 3 at threshold concentration for cleavage arrest (0.5 μM; E, F); to paclitaxel (5 μM; G, H). Time after fertilization (21 °C): (A, C, E, G) - 2.5 h; (B, D, F, H) – 6 h. Note the formation of a tuberculous egg (F) and a stabilized mitotic apparatus (light spots; G, H). The average embryo diameter is 115 μm.

noting that all tested molecules **1–25** exhibited comparable solubility in the assay system. Oxadiazole derivatives featuring both isothiazole (**5–8**) and aryl (**9–14**) pharmacophores as R^1 caused significant cleavage alteration, arrest and spinning comparable to the reference compounds (Table 1). Molecule **1** showed lower potency in our assay system. Moreover, at low concentrations it featured non-tubulin anti-proliferative activity whereas at higher concentrations (≥ 2 μM) it caused embryo abnormalities and embryotoxicity at later developmental stages. 1,3,4-Oxadiazole **3** ($R^2 = 4\text{-Cl-C}_6\text{H}_4\text{-NH-}$) afforded good activity (Fig. 1E, F). However, the product of respective reductive amination with 3-pyridylaldehyde **4** was considerably less active. Most active 1,3,4-oxadiazoles that affected tubulin polymerization were consistently substituted with a piperonyl- or ethylenedioxyphenyl moiety in the R^1 substituent (ex. **5–12**, Table 1). Replacement of these oxoaryl groups caused a deleterious effect on the activity of resulting compound (ex., molecules **7** and **8** vs **4**). For monosubstituted $R^2 = 4\text{-R-C}_6\text{H}_4\text{-NH-}$, where R = F, Me, CF$_3$, OCF$_3$ or disubstituted $R^2 = 3,4\text{-diF-C}_6\text{H}_4\text{-NH-}$, $3,4\text{-diCl-C}_6\text{H}_4\text{-NH-}$, $3\text{-Cl-4-OMe-C}_6\text{H}_4\text{-NH-}$ the respective 1,3,4-oxadiazole derivatives did not show any activity in the assay (% ITP = 20–30% at 10 μM) (data not shown [25]).

In general, a variety of substituents at R^1 were tolerated. For example, both unsubstituted anilines and their derivatives featured strong potency in vivo (Table 1, **9–12** and **13–14**). Isothiazole derivatives **5-8** displayed activities comparable to those of the respective phenyl derivatives **9–12**. For the "linear" derivatives of 1,3,4-oxadiazoles (**15–18**), substituents at R^1 reduced overall activity of the molecules. In addition, embryo abnormalities were observed for the compound **18** at concentrations ≥ 1 μM. An introduction of 3-(2-aminoquinoline) group at R^1 also resulted in a molecule **21** with reduced anti-tubulin activity.

Derivatives featuring pyrazole and imidazole rings at R^1 (**22–24**) showed no MT-based anti-proliferative activity, as concluded from both phenotype of exposed embryos and lack of embryo spinning. Molecule **21** was classified as a relatively weak tubulin modulator. Specifically, as evidenced from the detailed microscopy analysis it caused cleavage alterations and arrest with formation of tuberculous eggs typical of tubulin destabilizers. An unsubstituted pyrazole pharmacophore in R^1 position as in **25** led to a complete loss of anti-proliferative activity. Oxadiazole **19** lacking amine bridge was only marginally active in the sea urchin embryo assay (4 μM). Additional molecules featuring $R^2 = 4\text{-F-C}_6\text{H}_4\text{-NH-}$, $4\text{-Cl-C}_6\text{H}_4\text{-NH-}$, $4\text{-MeO-C}_6\text{H}_4\text{-NH-}$ and $3,4\text{-(OCH}_2\text{O)-C}_6\text{H}_4\text{-NH-}$, also displayed very low activity (data not shown).

Based on our in vivo data, we have selected the most active tubulin destabilizers represented by thiazole (**6**) and benzene (**12**) derivatives as well as their precursors **13** and **14**, and the non-tubulin anti-mitotic compound **1** as a comparator for further evaluations using in vitro tubulin polymerization and cell-based assays. Our rationale was to correlate the effects of lead candidates identified via the sea urchin embryo assay with the data generated by conventional studies of anti-tubulin activity. Biological activities of these agents were tested using four experimental approaches.

2.2.2. Cell growth inhibitory activity

First the inhibitory effect of selected compounds on proliferation of A549 lung carcinoma cells was determined with the MTT (3-(4,5-dimethylthiazol-2-yl)-2,5-diphenyltetrazolium bromide) cytotoxicity assay [26]. The IC$_{50}$ values for 1, 6, 12–14, and nocodazole are shown in Table 2.

Compounds containing benzene (**12**) and thiazole (**6**) rings demonstrated strong cytotoxicity comparable with nocodazole (Table 2). Analogues **13** and **14** lacking the –CH$_2$–Py moiety showed a markedly lower cell growth inhibitory effect. Reduced activity of these molecules could be attributed to their poor cell permeability. Compound **1** was inactive up to 20 μM concentration. We were unable to test higher concentrations of **1** due to its limited solubility in the cell culture medium.

2.2.3. Cell cycle arrest in G2/M

In our second approach, the ability of compounds **1, 6, 12–14** to alter A549 cell cycle progression was estimated by propidium iodide staining followed by flow cytometry analysis. The EC$_{50}$ values are shown in Table 2. Fig. 2 presents the detailed results of the DNA-based flow cytometric analysis of A549 cells for two lead molecules **6** and **12**, and nocodazole as a positive control. All three compounds induced concentration-dependent accumulation of cells in the G2/M phase, with **12** showing the strongest effect, followed by **6** and nocodazole (see also Table 2). Notably, both cell-based assays ranked the test articles similarly: cytotoxicity of oxadiazoles and their ability to induce G2/M arrest decreased in the following order: **12** > **6** > **14** > **13** > **1**.In both tests compound **1** did not produce an effect on A549 cell proliferation.

2.2.4. The effect on microtubule distribution in cells

In our third assay, we evaluated the effect of selected compounds on microtubule (MT) stability and distribution in cultured A549 cells. Cells were incubated with **1, 6, 12–14**, and nocodazole as a positive control. Then MTs were labelled by the indirect immunofluorescence method and analysed by fluorescence microscopy. 0.6% DMSO in water served as a control (Fig. 3)

Molecules **12** and **6** displayed the most pronounced MT disrupting effect of all molecules tested (Fig. 3C, D). Specifically, cells incubated with **12** did not feature microtubules as compared with nocodazole. Similarly, **6** ehxibited strong tubulin destabilizing effect, however small MT fragments were still discernable. Both **13** and **14** showed little or no effect on MT network at concentration of 5 μM (Fig. 3E, F). At higher concentrations (25 μM) these molecules did affect the MT network (Fig. 3G, H). Compound **1** did not affect the MTs in A549 cells even at the 20 μM concentration (not shown).

2.2.5. Inhibition of purified tubulin polymerization

Finally, we tested molecules prioritized by the in vivo experiments using in vitro tubulin polymerization assay. Specifically, purified bovine brain tubulin was polymerized in the presence of 10% DMSO followed by incubation with 10 μM of 1, 6, 12–14, nocodazole and additional 0.6% DMSO in water. Within 1 h post treatment, the resulting preparations were analysed by video-

Table 2
Cytotoxicity of Selected Oxadiazoles and their Effect on the Cell Cycle.

	DMSO[a]	Nocodazole[a]	1[b]	6	12	13	14
Cytotoxicity IC$_{50}$ $\pm$ SD, nM[c]	No effect	36.6 $\pm$ 5.8	>20,000	53.3 $\pm$ 11.5	15.0 $\pm$ 0.0	3000 $\pm$ 866	1566.6 $\pm$ 115.5
G2/M arrest EC$_{50}$ $\pm$ SD, nM[d]	No effect	106.5 $\pm$ 9.2	>20,000	63.0 $\pm$ 4.24	44.5 $\pm$ 0.7	8550 $\pm$ 353	2825 $\pm$ 318.2

[a] DMSO (0.4%) was used as a negative control, and nocodazole as a positive control.
[b] At concentrations higher than 20 μM compound **1** formed crystals.
[c] Average of three experiments.
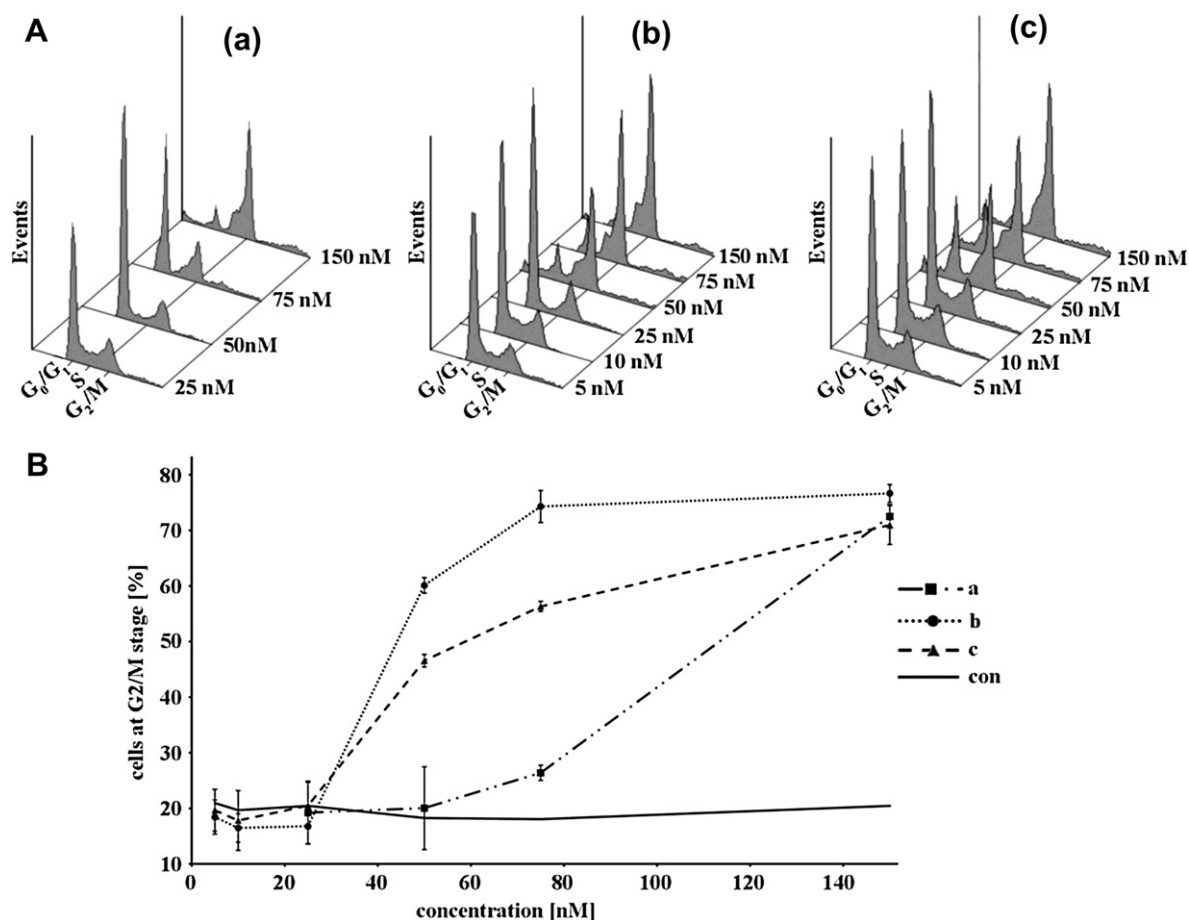[d] Average of two experiments.

Fig. 2. The effect of selected oxadiazoles on A549 cell cycle. (A) DNA-based flow cytometry histograms of nocodazole (a), 12 (b), and 6 (c). (B) A concentration-dependent cell cycle arrest in the G2/M phase caused by nocodazole (a), 12 (b), and 6 (c). 0.4% DMSO in water was used as a control.

enhanced contrast differential interference contrast (VEC-DIC) microscopy (Fig. 4).

As shown on Fig. 4, molecule **12** completely inhibited the MT assembly, this effect being more profound than that of nocodazole. Specifically, samples treated with **6** displayed more aggregates or short MT's than nocodazole. For the compound **14**, a number of depolymerized MT's have been detected, albeit the effect was moderate compared to both **12** and nocodazole. Molecule **13** exerted only marginal effect on MT dynamics.

Both cell-based and *in vitro* MT assays converged on the molecule **12**. This agent consistently featured the highest activity when compared with nocodazole. Compound **6** demonstrated strong tubulin destabilizing effect as well. Analogs **13** and **14** were less active, while compound **1** characterized as non-tubulin agent by sea urchin embryo assay failed to depolymerize MT's both in whole cells and *in vitro*. Data generated by the cell culture assays correlated well with the results of the sea urchin embryo studies. Specifically, derivatives of oxadiazoles endowed with benzene substituents (*ex.*, **12**) were the most potent. Replacement of the –CH$_2$–Py moiety (**13** and **14**) led to both decreased anti-proliferative activity in A549 cells as well as to a weaker tubulin destabilizing properties *in vivo* and *in vitro*. The ability of **13** and **14** to produce cleavage alteration/arrest at nanomolar concentrations could be explained by the high frequency of cell divisions that occur every 35–40 min at early stages of the sea urchin embryo development. Oxadiazoles containing isothiazole moiety (*ex.*, **6**) displayed comparable activity across the assay panel. In contrast to **13**

and **14**, in these series the absence of –CH$_2$–Py group (*ex.*, **1**) yielded complete loss of the MT destabilizing effect. Respective pyrazole or imidazole derivatives (**22–24**) showed significant non-tubulin antimitotic activity.

2.2.6. Computational studies of 1,3,4-oxadiazole derivatives

To rationalize the tubulin activity of 1,3,4-oxadiazole derivatives, we conducted a series of three-dimensional (3D) similarity comparisons [27]. These studies utilized reference compounds that were docked into the colchicine binding site at the interface of α/β tubulin subunits. The reference set comprised: i) known tubulin binders colchicine and its sulfur analogue DAMA-colchicine [11], podophyllotoxin [11], nocodazole [5,6], CA-2, CA-4 [28], and taxol [10]; ii) compounds with unknown binding site, namely indibulin [29] and benzoquinolizidine [30] (chemical structures provided in the Supporting Information, Fig. S1). A pool of conformers from the reference set was generated using Omega [31] and ROCS [32] (both from OpenEye Scientific Software Ltd). It was further used to select poses matching the reported co-crystal structure of colchicine and tubulin. This procedure was repeated for benzoquinolizidine, indibulin and oxadiazole series although there were no data suggesting that these molecules bind tubulin at the colchicine binding site. Previous work showed that combretastatins compete for tubulin binding with colchicines. This data suggest overlapping binding sites for these molecules [28,33]. ROCS results implied that two compounds (**13** and **14**) had higher similarity to **CA-2** and **CA-4** (Table 3).
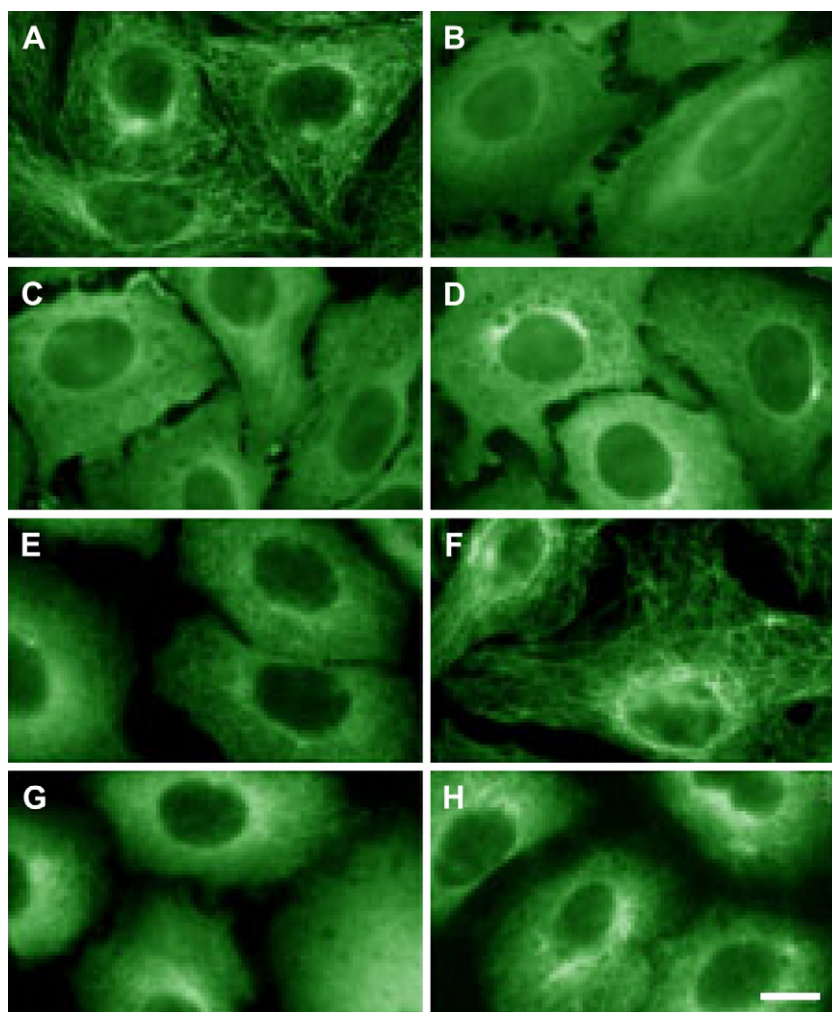
Fig. 3. Effect of selected compounds on the MT networks in A549 lung carcinoma cells analysed by indirect immunofluorescence microscopy. Cells were treated with 0.6% DMSO in water: (A) as a negative control, with 5 μM of nocodazole as positive control (B), and following test compounds for 8 h: 12 (5 μM, C), 6 (5 μM, D), 14 (5 μM, E; 25 μM, G), 13 (5 μM, F; 25 μM, H). Bar: 20 μm.

Molecules **6** and **12** were also potent MT dynamics inhibitors in the biological assays. However, their similarity score was affected by bulky substituents absent in combretastatins (Fig. 5).

Because ROCS is a ligand-based tool that does not take into account protein constraints, compound **12** appeared to be misaligned in relation to other molecules featuring 4-Py–CH$_2$ substituent. Several studies suggested this substitution region to be unfavorable due to its steric clash with amino acid residues of the tubulin binding pocket (reviewed in [19]). We concluded that the inverted alignment of **12** could yield better fitting yielding high ROCS similarity scores (0.99 *vs* **CA-2**, and 0.95 *vs* **CA-4**, respectively). Black arrows in Fig. 5 indicate potential H-bond donors. The aromatic rings were out-of-plane (twisted) due to the mismatch between amine and vinyl spacer groups (orange arrow in Fig. 5) reducing the overall similarity score of this dataset. Considering tubulin activity of the studied molecules, we concluded that this slight twisting of the aromatic rings was tolerated. The binding mode for **6** and **12** matched the consensus pharmacophore derived from a set of tubulin inhibitors that bind the colchicine site [34]. Blue and black arrows show superposition of hydrophobic and hydrogen bonding interactions, respectively. Orange arrow indicates mismatch of the spacer group. Labels A and B in **11** illustrate overlapping rings of CA-2 and this oxadiazole derivative. Carbon

colors: combretastatin A-2 (green), docked compounds (gray). Oxygen, nitrogen, sulfur and hydrogen are red, blue, yellow and white, respectively. Non-polar hydrogens were omitted for the sake of clarity.

Following the reported SAR data for combretastatin derivatives [19,35] we propose that the aniline linker bridge affects the alignment of phenyl rings and keeps them oriented in a twisted manner similar to other tubulin inhibitors (Fig. 6) [36].

In order to rationalize the observed SAR, we further docked several representative molecules (**1**, **4**, **7**, **12**, Fig. 6) into the tubulin cavity (PDB ID **1SA0**) using FRED [37]. These molecules appeared to bind in a specific manner, fitting R^2 moiety (Table 1) into the deepest region of tubulin cavity, while the oxadiazole and R^1 substituents were oriented towards the cavity entrance.

In our hands, data for cytotoxicity, G2/M arrest, MT polymerization and the sea urchin embryo assays converged on **12** as a molecule with the activity profile similar to nocodazole. It was followed by compounds **6**, **14** and **13** in the decreasing order of potency. Compound **1** was inactive in most of the assays, as it did not display anti-tubulin properties. The molecule did cause cleavage arrest in sea urchin embryo. However, this activity was likely driven by a non-tubulin mechanism as suggested in the literature for several CA analogues with low anti-tubulin activity
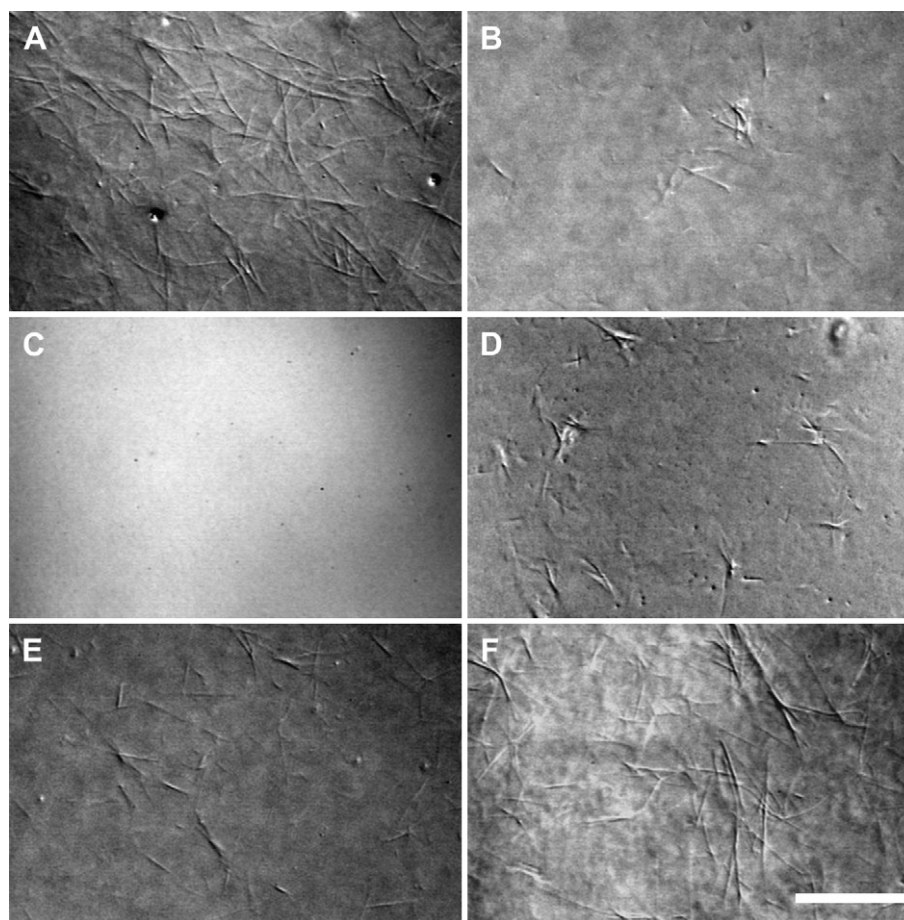
Fig. 4. Effect of selected compounds on purified tubulin assembly *in vitro* analysed by VEC-DIC microscopy. Samples treated with additional 0.6% DMSO in water as a negative control (A) showed single MTs. Samples treated with 10 μM of nocodazole (B), 12 (C), 6 (D), 14 (E) or 13 (F) showed lack of intact MTs of MT bundles. Bar: 17 μm.

[28]. Lack of the dioxolane moiety in R^2 was detrimental to the antimitotic activity of molecules (compare **4**, **7** and **8**, Table 1). In analyzing results of the docking studies, we reasoned that the dioxolane group of **7** and **12** potentially overlapped with the trimethoxy substituents of both colchicine and CA-2. The binding mode for **4** was likely inverted. None of the identified positions provided reasonable overlap of the *para*-chlorophenyl group with the trimethoxyphenyl substituent of CA-4 (Fig. 6). Direct linking of the phenyl rings in CA-4 derivatives reduced the activity of these molecules. This finding suggests potential steric hindrance at the inner part of colchicine binding site of tubulin, where the R^2 group is likely to bind. Moreover, our earlier report showed that the hydrogen bond acceptor at *para* position was critical to the antimitotic activity [36].

Docking poses further suggested a potential hydrogen bond between the *Cys*238 and the dioxolane ring (Fig. 6). As opposed to the strict steric requirements for R^2, the substitution pattern of R^1 pharmacophore was less restrictive. As seen in Table 1, all potent compounds featured diverse substituents at the R^1 position. Both isothiazole as well as phenyl moieties were well tolerated. Notably, pyrrole or imidazole analogues **22**, **23**, **24** displayed marginal activity in our assays, suggesting unfavorable interaction(s) with the colchicine binding site. *Ortho*-anilines with or without N-substituent were consistently active as well. Methoxylation of the core ring reduced overall potency (compare compounds **13**, **16** and **17**; **14** and **15**) presumably due to the steric hindrance between R^2 and amino acid residues of tubulin. Replacement of pyridine group with isothiazole in R^1 reduced potency of the resultant compound

20, probably because of a mismatch between this group and the hydrophobic pocket in tubulin. Compound **18** was a weak tubulin inhibitor despite of its favorable substitution with the 3,4,5-trimethoxyphenyl group in R^1 (*ex.*, A-ring in combretastatins). This outcome is likely due to the lack of spacer between R^1 and oxadiazole core causing steric clash between the molecule and the inner part of the pocket [35].

ROCS data further suggested that the inactive compound **1** was in the same range of similarity with other molecules from the set. Docking experiments with **1** placed its oxadiazole group in the same orientation as A-ring of CA-4 and CA-2. This is an unfavorable binding mode as the oxadiazole moiety is deeply buried into the binding site (Fig. 6). We have observed similar behavior for the compounds **21** and **25** both featuring unsubstituted amines. Unfortunately, we were unable to identify a low energy minimum conformation (< -75 kcal mol^{-1}) for the active compounds **13** and **14** to rationalize their binding mode to tubulin.

Table 3
3D similarity scores for selected ligands to **CA–2** and **CA–4**.[a]

Compound	CA-2	CA-4
13	1.39	1.32
14	1.35	1.32
17	1.28	1.15
1	1.28	1.21
6	1.01	0.98
12	0.99	0.98

[a] ROCS results were based on the shape and color (electrostatics) similarity score. See Supporting Information, Fig. S2.

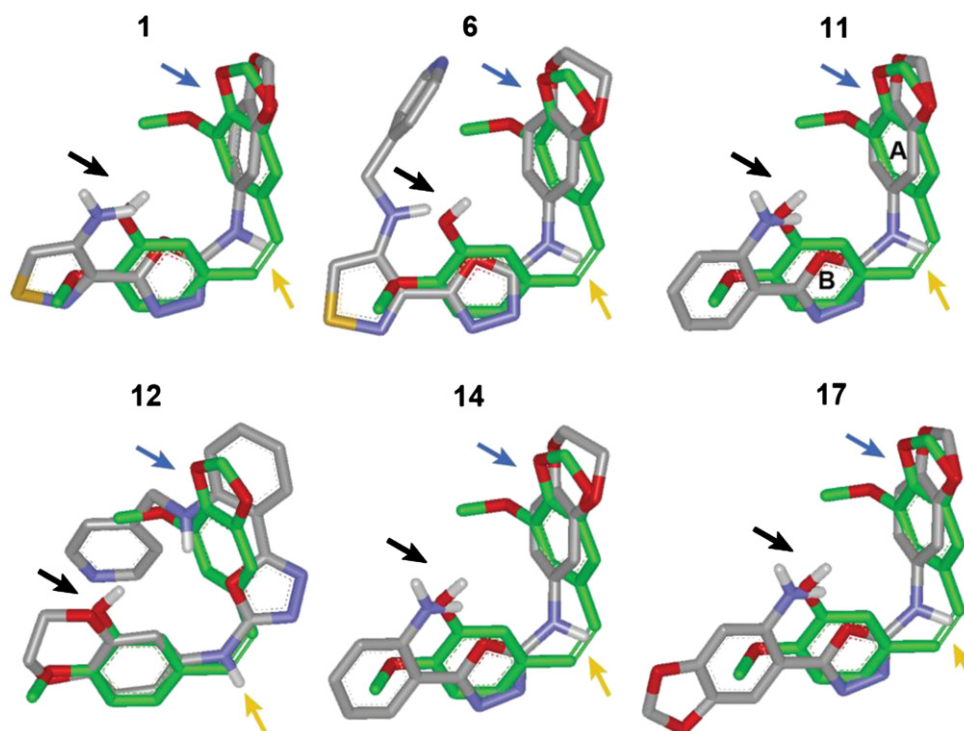**Fig. 5.** Superposition of selected compounds to CA-2 by ROCS.
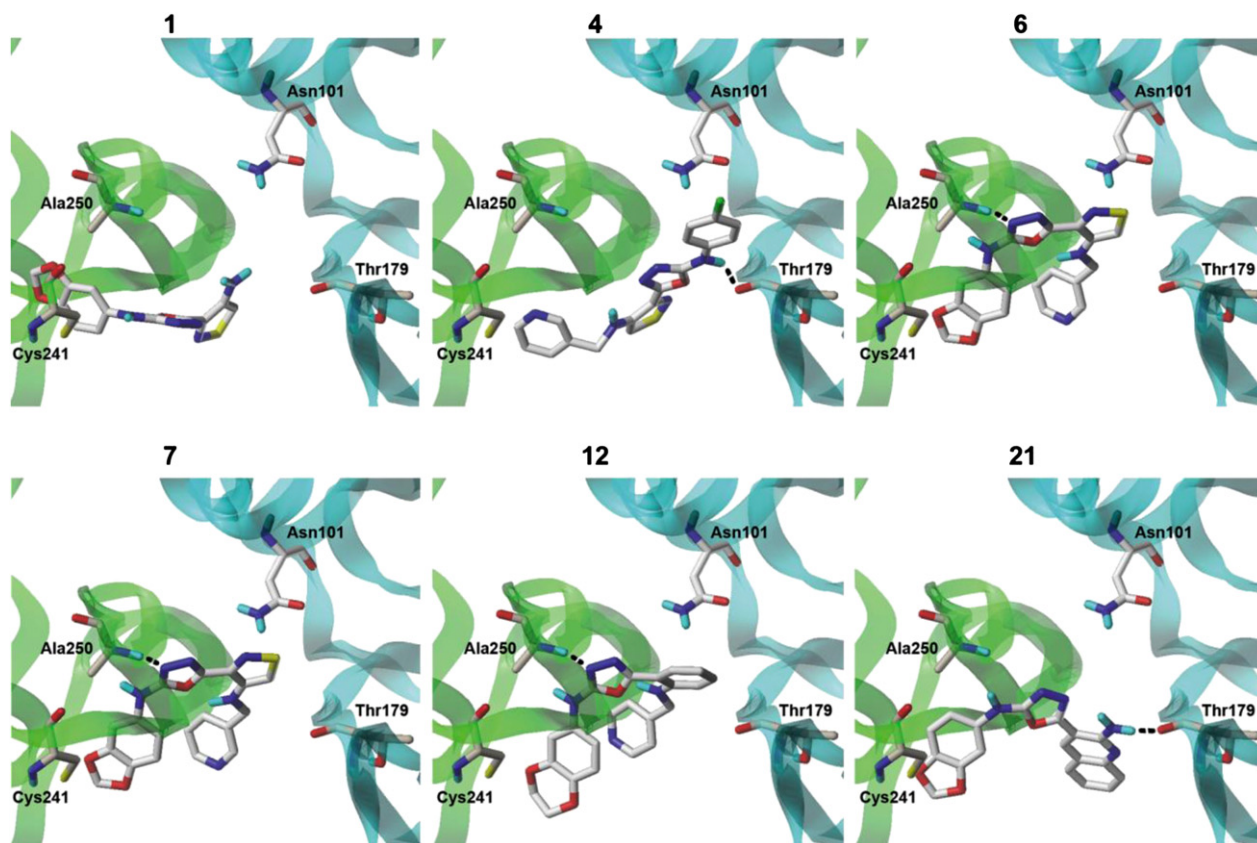

Fig. 6. Docking results for binding of selected 1,3,4-oxadiazoles (1, 4, 6, 7, 12 and 21) to α- and β-subunits of tubulin. View from the pocket entrance. Tubulin structure is represented as cyan (α-subunit) and light green (β-subunit) ribbons. Some amino acid side chains are shown. Dashed lines represent the key hydrogen bonds.

3. Conclusions

A series of novel 1,3,4-oxadiazole derivatives based on structural and electronic overlap with combretastatin A-2 have been designed, synthesized and tested *in vivo* using the sea urchin embryo development assay. We monitored the effects of these agents on two specific developmental stages of the embryo, namely i) fertilized egg to assess anti-mitotic activity; ii) free-swimming blastulae to detect behavioral changes in the embryo swimming pattern. These were quantified by a threshold concentration resulting in respective abnormalities allowing for both rapid prioritization of the tubulin inhibitors and identification of non-specific cytotoxic substances. Following the sea urchin embryo studies, the prioritized actives were further profiled in a panel of cell-based and *in vitro* assays. Further evaluation of microtubule and cell cycle effects yielded lead molecules **6** and **12** with activity profiles similar to that of nocodazole. Specifically, these compounds featured considerable anti-mitotic effect with EC values of 0.5–5 nM in the sea urchin embryo based on the tubulin destabilizing effect. Molecules **6** and **12** were further confirmed to be equipotent to nocodazole in their ability to depolymerize MT both *in vitro* and in the intact cells. Similar to nocodazole, compounds **6** and **12** afforded pronounced cytotoxicity (IC_{50} = 53 and 15 nM, respectively) and cell cycle arrest in G2/M phase (EC_{50} = 63 and 45 nM, respectively) in cultured A549 human lung carcinoma cells. A combination of the sea urchin embryo assay with the tests of tubulin dynamics in cultured human tumor cells allowed for the rapid identification and prioritization of promising and specific MT inhibitors from a novel chemical class. SAR data for 1,3,4-oxadiazoles were further aligned with results of computational studies. Several identified actives were superimposed to CA-4 and CA-2 molecules and docked into the colchicine binding site of tubulin. Docking results were used to propose the putative mode of binding for these novel molecules.

4. Experimental section

4.1. Chemistry

NMR data were collected on a Bruker DR-500 instrument (working frequencies of 500.13 MHz (1H)). Mass spectra were collected on a Finningan MAT/INCOS 50 instrument (70 eV) using direct probe injection.

4.2. 4-Aminoisothiazolecarboxylic-3-acid hydrazide

A mixture of amide of 4-aminoisothiazole-3-carboxylic acid [38] (5.39 g; 38 mM) and 28 mL of 85% hydrazine hydrate was refluxed for 3 h and cooled to RT. The resulting precipitate was filtered off, washed with ice water (3 × 5 mL) and dried *in vacuo* to furnish acyl hydrazide (4.17 g, 70% yield), mp 170–172 °C. ^{1}H NMR (DMSO-d_6, δ): 4.45 (s, 2H, NH$_2$), 5.72 (s, 2H, NH$_2$), 7.68 (s, 1H), 9.7 (br.s, 1H, NH).

4.2.1. Preparation of 5-(arylamino)-1,3,4-oxadiazoles from acid hydrazides and arylisothiocyanates (general procedure 1)

A solution (or suspension) of acyl hydrazide and arylisothiocyanate(1 mM each) in *t*BuOH (3 mL) was refluxed for 10 min followed by a vigorous stirring for 1 h at 50–60 °C. The reaction mixture was concentrated *in vacuo* and the residue was treated with MeCN (5 mL). DCC (1.5 mM) was added to the resulting suspension, the mixture was stirred at reflux for 3 h and cooled to RT. The precipitate was filtered off, washed with hot benzene or hot MeCN (2 × 2 mL) and dried.

4.2.2. 2-(4-Aminoisothiazolyl-3)-5-((3,4-methylenedioxy)phenyl)amino-1,3,4-oxadiazole **1**

It is prepared from hydrazide of 4-aminoisothiazole carboxylic-3-acid and 3,4-methylenedioxyphenylisothio cyanate as described in procedure 1: 80% yield, mp 268–270 °C. ^{1}H NMR (DMSO-d_6, δ): 5.81 (s, 2H, NH$_2$), 6. 00 (s, 2H, OCH$_2$O), 6.93 (d,J = 8.7 Hz, 1H), 7.04 (d, J = 8.7 Hz, 1H), 7.29 (s,1H), 7.80 (s, 1H), 10.78 (s, 1H, NH). ^{13}C NMR (DMSO-d_6, δ): 97.5, 101.4, 101.7, 110.3, 125.2, 133.7, 138.8, 142.2, 148.0, 148.2, 158.1, 166.7. Mass-spectrum: EI-MS (70 eV, 20 °C) (*m/z*, *I*, %): 303 [M]$^+$ (100), 162 (54), 125 (52). Anal. Calcd for C$_{12}$H$_9$N$_5$O$_3$S: C, 47.52; H, 2.99; N, 23.09; S 10.57. Found: C, 47.22; H, 3.03; N, 22.87; S 10.70.

4.2.3. 2-(4-Aminoisothiazolyl-3)-5-((3,4-ethylenedioxy)phenyl)amino-1,3,4-oxadiazole **2**

It is prepared from the hydrazide of 4-aminoisothiazolecarboxylic-3-acid and 3,4-ethylenedioxyphenylisothiocyanate according to procedure A: 69% yield, mp 265–267 °C. ^{1}H NMR (DMSO-d$_6$, δ): 4.23 (m, 4H, OCH$_2$CH$_2$O), 5.83 (s, 2H, NH$_2$), 6.86 (d,J = 8.7 Hz, 1H), 7.00 (dd, J_1 = 8.7 Hz, J_2 = 2.5 Hz, 1H), 7.24 (d, J = 2.5 Hz, 1H), 7.79 (s, 1H), 10.80 (br.s, exch. D$_2$O, 1H, NH). EI-MS (*m/z*, *I*, %): 317 [M]$^+$. Anal. Calcd for C$_{13}$H$_{11}$N$_5$O$_3$S: C, 49.20; H, 3.49; N, 22.07; S 10.11. Found C, 48.94; H, 3.51; N, 21.95; S 9.75.

4.2.4. 2-(4-Aminoisothiazolyl-3)-5-(4-chloro)phenylamino-1,3,4-oxadiazole **3**

It is prepared from hydrazide of 4-aminoisothiazolylcarboxylic-3 acid and 4-chlorophenylisothiocianate according to the procedure 1, yield 56%, mp 211–213 °C. ^{1}H NMR (DMSO-d_6, δ): 5.85 (s, 2H, NH$_2$), 7.44 (d, J = 8.6 Hz, 2H), 7.63 (d, J = 8.6 Hz, 2H), 7.8 (s, 1H), 11.1 (br.s, exch. D$_2$O, 1H, NH). EI-MS (*m/z*, *I*, %): 295 [M]$^+$ (27), 293 [M]$^+$ (63), 127 (49), 125 (100). Anal. Calcd for for C$_{11}$H$_8$ClN$_5$OS: C, 44.98; H, 2.75; N, 23.84; Cl 12.07; S 10.92. Found: C, 45.30; H, 2.96; N, 23.51; Cl 12.02; S 11.06.

4.2.5. N-(4-chlorophenyl)-5-{4-[(pyridin-3-ylmethyl)amino]isothiazol-3-yl}-1,3,4-oxadiazol-2-amine **4**

Solution of of 4-aminoisothiazole-3-carboxamide (0.715 g; 5 mM), 3-pyridylaldehyde (0.696 g; 6.5 mM) and *p*TsOH (20 mg) in a mixture of MeOH (1.5 mL) and MeCN (6 mL) was stirred for 48 h at RT. The mixture was concentrated *in vacuo* and treated with *t*BuOMe (5 mL). The precipitate was filtered, washed with a mixture of *t*BuOMe-hexanes (1:1) and dried to furnish a pale yellow crystals of the Schiff base (0.901 g, 78%). EI-MS (*m/z*, *I*, %): 232 [M]$^+$ The material was used in the next step without further purification. NaBH$_4$ (0.28 g; 7.5 mM) was added portion-wise (15 min) to the solution of the Schiff base (0.9 g, 3.9 mM) in MeOH (6 mL) under vigorous stirring at RT. After the addition was completed, the reaction mixture was stirred for additional 30 min and concentrated *in vacuo*. The residue was triturated with water, pH was adjusted to 9 with AcOH, the mixture was extracted with *t*BuOMe (5 × 20 mL), the organic phase was collected and concentrated *in vacuo* and evaporated. The solid material was dried with heating *in vacuo* (P$_2$O$_5$) to afford the target carboxamide as a pale yellow crystals (0.90 g, 98.7% yield), m.p. 135–137°. EI-MS (*m/z*, *I*, %): 234 [M]$^+$.

4.2.6. 4-[(pyridin-3-ylmethyl)amino]isothiazole-3-carbohydrazide

A mixture of 4-((3-pyridyl)methyl)4-aminoisothiazole-3-carboxamide (0.89 g; 3.8 mM) and 85% hydrazine hydrate (6 mL) was refluxed for 2 h. Excess of hydrazine was removed *in vacuo* followed by co-evaporation with *i*PrOH. The resulting oil was further dried *in vacuo* with heating under P$_2$O$_5$ to furnish 4-((3-pyridyl)methyl)aminoisothiazol-3-carbohydrazide (0.92g, 97%yield) as a viscous oil (Rf 0.22, EtOAc–MeOH = 19:1). This material was used

in the next step without further purification. The target compound **4** was prepared from the 4-[(pyridin-3-ylmethyl)amino]isothiazole-3-carbohydrazide (0.25 g; 1 mM) and 4-Cl-phenyl-isothiocyanate (1.2 mM) as described in the procedure 1, yield 0.163 g (50%), mp 244–246°. ^{1}H NMR (DMSO-d_6, δ): 4.5 (d, *J* = 6 Hz, 2H, CH$_2$), 6.75 (t, *J* = 6 Hz, 1H, *NH*), 7.35 (dd, *J*$_1$ = 7.5 Hz, *J*$_2$ = 5 Hz, 1H, 3-Py), 7.44 (d, *J* = 8.3 Hz, 2H, Ar), 7.64 (d, *J* = 8.3 Hz, 2H, Ar), 7.78 (s, 1H, isothiazole), 7.8 (d, *J* = 5 Hz, 1H, 4-Py), 8.48 (d, *J* = 7.5 Hz, 1H, 2-Py), 8,62 (s, 1H, 2-Py), 11.13 (br.s., exch. D$_2$O, 1H, NH). ^{13}C NMR (DMSO-d$_6$, δ): 48.3, 118.0, 123.9, 124.2, 126.7, 129.0, 133.7, 134.8, 135.6, 138.3, 141.5, 148.6, 148.9, 158.0, 166.8. EI-MS (*m/z*, *I*, %): 384 [M]$^+$, 386 [M]$^+$. Anal. calcd for C$_{17}$H$_{13}$ClN$_6$OS: C, 53.06; H, 3.40; N, 21.84; S 8.33. Found: C, 53.17; H, 3.55; N, 21.95; S 8.56.

4.2.7. 2-((4-((Pyridyl-4)methyl)amino)isothiazolyl-3)-5-(3,4-ethylenedioxy)phenylamino-1,3,4-oxadiazole **6**

A mixture of 4-aminoisothiazole-3-carboxamide [38] (3.44 g; 24 mM), 4-pyridylaldehyde (3.08 g; 28.8 mM) in MeOH (10 mL), MeCN (25 mL) and *p*TsOH (100 mg) was stirred 5 h at RT. The precipitate of Schiff base was filtered off, washed with MeCN (5 mL) dried, and reduced with NaBH$_4$ without further purification as follows. To the suspension of Schiff base (4.9 g; 21.1 mM) in *i*PrOH (50 mL) was added NaBH$_4$ (2.28 g; 60 mM) in three portions with stirring and reflux for 7 h. The reaction mixture was concentrated *in vacuo* to 1/4 of the original volume. The residue was triturated with water, AcOH was added to pH 9, the precipitate was filtered off, washed with ice water and dried. The resulting amine (2.37 g) and NH$_2$NH$_2$·H$_2$O (17 mL) were refluxed for 3.5 h, the mixture was cooled to RT, the precipitate was filtered off, washed with ice water (2 × 3 mL) and dried to afford 4-((4-pyridyl)methyl)aminoisothiazol-3-carbo-hydrazide in a 59% total yield (3 steps starting from 4-amino-isothiazole-3-carboxamide), mp 146–148 °C. The material was used in the next step without further purification. The hydrazide (1.5 g; 6 mM) and 3,4-ethylenedioxyphenylisothiocyanate were reacted as described in the procedure 1 to yield **6**, 75%, mp 255–258 °C. ^{1}H NMR (DMSO-d$_6$, δ): 4.24 (m, 4H, OCH$_2$CH$_2$O), 4.53 (d, *J* = 6.1 Hz, 2H), 6.83 (t, *J* = 6.1 Hz, 1H, NH), 6.84 (d, *J* = 8.7 Hz, 1H), 7.00 (dd, *J* = 8.7 Hz, *J* = 2.5 Hz, 1H), 7.25 (d, *J* = 2.5 Hz, 1H), 7.37 (d, *J* = 5.5 Hz, 2H), 7.62 (s, 1H), 8.52 (d, *J* = 5.5 Hz, 2H), 10.72 (s, 1H, NH). ^{13}C NMR (DMSO-d$_6$, δ): 48.7, 69.4, 107.1, 112.0, 115.3, 126.5, 129.4, 133.6, 138.4, 138.8, 141.7, 144.6, 148.2, 149.1, 158.2, 166.5. EI-MS (*m/z*, *I*, %): 408 [M]$^+$ (63), 233 (66), 216 (49), 176 (84), 151 (77), 120 (85), 92 (100). Anal. Calcd for C$_{19}$H$_{16}$N$_6$O$_3$S: C, 55.87; H, 3.95; N, 20.58; S 7.85. Found: C, 56.09; H, 3.91; N, 20.45; S 8.12.

4.2.8. Reductive amination of heterocyclic amines with aldehydes (general procedure 2)

A suspension of amine (1 mM), pyridyl aldehyde and *p*TsOH (0.1 mM) in dry MeCN (5 mL) was placed in a flask equipped with addition funnels and a pressure equalizing sleeve filled with 4 Å molecular sieves. The resulting mixture was refluxed with stirring for 3 h and cooled to RT. The precipitate of a Schiff base was filtered, dried and reduced with NaBH$_4$ without further purification. NaBH$_4$ (3 mM) was added to the suspension of Schiff base in *i*PrOH (5 mL) and the resulting mixture was refluxed for 3h with stirring. Subsequently, *i*PrOH was removed *in vacuo*, the residue was treated with water. The resulting crystals were filtered off, washed with aqueous 5% AcOH, water and dried.

4.2.9. 2-((4-((Pyridyl-3)methyl)amino)isothiazolyl-3)-5-(3,4-methylenedioxy)phenylamino-1,3,4-oxadiazole **7**

It is prepared from 2-((4-amino)isothiazolyl-3)-5-(3,4-meth-ylenedioxyphenyl)amino-1,3,4-oxadiazole (3) and 3-pyr-idinecarbaldehyde according to procedure 2, 88% yield, mp 230–232 °C. ^{1}H NMR (DMSO-d$_6$, δ): 4.50 (d, *J* = 6.1 Hz, 2H), 6.00 (s, 2H,

OCH$_2$O), 6.75 (t, *J* = 6.1 Hz, 1H, NH), 6.92 (d, *J* = 8.7 Hz, 1H), 7.10 (d, *J* = 8.7 Hz, 1H), 7.30 (s, 1H), 7.37 (dd, *J* = 7.8 Hz, *J* = 5.0 Hz, 1H), 7.75 (s, 1H), 7.80 (d, *J* = 7.8 Hz, 1H), 8.47 (d, *J* = 5.0 Hz, 1H), 8.63 (s, 1H), 10.80 (br.s, 1H, NH). ^{13}C NMR (DMSO-d$_6$, δ): 49.0, 97.7, 100.6, 101.8, 111.3, 123.3, 123.4, 126.4, 133.9, 135.2, 138.0, 141.9, 147.8, 148.2, 148.6, 148.9, 158.4, 166.6. EI-MS (*m/z*, *I*, %): 394 [M]$^+$ (42), 162 (79), 137 (71), 92 (100). Anal. Calcd for C$_{18}$H$_{14}$N$_6$O$_3$S: C, 54.81; H, 3.58; N, 21.31; S 8.13. Found: C, 55.00; H, 3.69; N, 21.05; S 7.96.

4.2.10. 2-((4-((Pyridyl-3)methyl)amino)isothiazolyl-3)-5-(3,4-ethylenedioxy)phenylamino-1,3,4-oxadiazole **8**

It is prepared from 2-((4-amino)isothiazolyl-3)-5-(3,4-ethyl-enedioxy)phenylamino-1,3,4-oxadiazole **2** and 3-pyridinecarbal-dehyde according to procedure 2, 84% yield, mp 226–228 °C. ^{1}H NMR (DMSO-d$_6$, δ): 4.24 (m, 4H, OCH$_2$CH$_2$O), 4.53 (d, *J* = 6.0 Hz, 2H), 6.75 (t, *J* = 6.0 Hz, 1H, NH), 6.85 (d, *J* = 8.7 Hz, 1H), 7.00 (d, *J* = 8.7 Hz, 1H), 7.22 (s, 1H), 7.36 (dd, *J* = 7.8 Hz, *J* = 5.0 Hz, 1H), 7.75 (s, 1H), 7.80 (d, *J* = 7.8 Hz, 1H), 8.45 (d, *J* = 5.0 Hz, 1H), 8.64 (s, 1H), 10.72 (br.s, 1H, NH). EI-MS (*m/z*, *I*, %): 408 [M]$^+$ (31), 176 (37), 151 (89), 92 (100). Anal. Calcd for C$_{19}$H$_{16}$N$_6$O$_3$S: C, 55.87; H, 3.95; N, 20.58; S 7.85. Found: C, 56.20; H, 4.14; N, 20.32; S 7.99.

4.2.11. 2-((4-((Pyridyl-4)methyl)amino)isothiazolyl-3)-5-(3,4-methylenedioxy)phenylamino-1,3,4-oxadiazole **5**

It is prepared from 2-((4-amino)isothiazolyl-3)-5-(3,4-methyl-enedioxy)phenylamino-1,3,4-oxadiazole **1** and 4-pyridinecarbal-dehyde according to procedure 2, 84% yield, mp 252–255 °C. ^{1}H NMR (DMSO-d$_6$, δ): 4.51 (d, *J* = 6.0 Hz, 2H), 6.00 (s, 2H, OCH$_2$O), 6.82 (t, *J* = 6.1 Hz, 1H, NH), 6.93 (d, *J* = 8.7 Hz, 1H), 7.05 (d, *J* = 8.7 Hz, 1H), 7.31 (s, 1H), 7.38 (d, *J* = 5.5 Hz, 2H), 7.64 (s, 1H), 8.50 (d, *J* = 5.5 Hz, 2H), 10.81 (s, 1H, NH). EI-MS (*m/z*, *I*, %): 394 [M]$^+$ (100), 216 (38), 162 (50), 161 (47), 92 (46). Anal. Calcd for C$_{18}$H$_{14}$N$_6$O$_3$S: C, 54.81; H, 3.58; N, 21.31; S 8.13. Found: C, 54.71; H, 3.70; N, 21.15; S 8.05.

5. Both synthetic protocols and analytical data for compounds 9–25 are summarized in the supporting information

5.1. Biology

5.1.1. Sea urchin embryo assay

Adult sea urchins *Paracentrotus lividus* were collected from Mediterranean Sea at Cyprus coast and kept in an aerated seawater tank. Gametes were obtained by intracoelomic injection of 0.5 M KCl. Eggs were washed with filtered sea water and fertilized by adding drops of a diluted sperm. Embryos were cultured at room temperature under gentle agitation with a motor-driven plastic paddle (60 rpm) in filtered sea water. The embryos were observed with a light microscope Biolam (LOMO, S.-Peterburg, Russia). For treatment with the test compounds, 5 mL aliquots of embryo suspension were transferred to 6-well plates and incubated as a monolayer at a concentration up to 3000 embryos/mL. Stock solutions of compounds were prepared either in 95% EtOH at 5 mM or in DMSO at 5–10 mM concentrations followed by a 10-fold dilution with 95% EtOH. The anti-proliferative activity was assessed by exposing fertilized eggs (10–25 min after fertilization, 45–60 min before the first mitotic cycle completion) to 2-fold decreasing concentrations of the compound. Cleavage alteration and arrest were clearly detected at 2.5–6 h after fertilization (Fig. 1). The effects were quantitatively estimated as a threshold concentration resulting in cleavage alteration and embryo death before hatching or full mitotic arrest. For tubulin destabilizing activity, the compounds were tested on free-swimming blastulae just after

hatching (9–12 h after fertilization), originated from the same embryo culture. Embryo spinning was observed after 0.5–20 h of treatment, depending on the nature and concentration of the compound. Both spinning and lack of forward movement were interpreted to be the result of the tubulin destabilizing activity of a molecule according to previous studies [21,22].

5.1.2. Cell culture

A549 human lung epithelial carcinoma cells (CCL-185™) were cultured with Dulbecco's Modified Eagle medium (DMEM) containing 10% fetal bovine serum and 1% antibiotic penicillin/streptomycin at 37 °C under a 5% CO_2 humidified atmosphere.

5.1.3. MTT cytotoxicity assay

Cells were seeded in 96-well plates at a density of 3×10^3 cells per well. Stock solutions of test compounds were prepared in dimethylsulfoxide (DMSO). Cells were treated for 24 h with 6 and 12 at 0.001–0.3 μM, 13 and 14 at 0.5–25 μM, 1 at 1–20μM, or with nocodazole at 0.001–0.3 μM as a positive control (8 wells per each concentration value). DMSO (0.4%) served as a control. The number of surviving cells was determined by the colorimetric MTT assay [26]. MTT (3-(4,5-dimethylthiazolyl-2)-2,5-diphenyl-2H-tetrazoliumbromid, Roth GmbH, Karlsruhe, Germany) was prepared at 5 mg/mL in phosphate buffer saline (PBS) and filtered through a 0.22 μm filter. 20 μL sterile MTT solution (final concentration 0.5 mg/mL) was added to each well 2 h before the end of compound exposure. Then the supernatant was removed, and 100 μL DMSO containing 10% SDS and 0.6% acetic acid was added to each well. Resulting formazan crystals were solubilised by thorough mixing on a plate shaker. Optical density was measured at 590 nm with 690 nm reference filter using EL808 Ultra Microplate Reader (Bio-Tek Instruments, Winooski, USA). Experiments for all compounds were repeated 3 times and IC_{50} values were determined by sigmoidal curve fitting using Excel-based software.

5.1.4. Cell cycle analysis

A549 cells were seeded at a density of 5×10^5 cells in 50 mm culture dishes, treated with test compounds at concentrations of 0.001–25 μM for 24 h and harvested by trypsinization. Nocodazole and 0.4% DMSO served as positive and negative controls, respectively. After centrifugation (1000 rpm, 25 °C, 5 min) and resuspension in HBS (14 mM HEPES, pH 7.4, 0.9% NaCl₂) cells were fixed by dropwise adding to 70% ethanol (−20 °C). Fixed cells were centrifuged (1300 rpm, 4 °C, 10 min) and treated with 1 mg/mL RNase in HBS (Sigma, St. Louis, USA) for 30 min at 37 °C, followed by incubation with 50 μg/mL propidium iodide in PBS (Roth, Karlsruhe, Germany) for 30 min at 37 °C. The DNA content of a total of 10000 cells in each sample was analysed using an Epics Altra flow cytometer (Beckman Coulter, Germany). Experiments for all compounds were repeated 2 times, and EC_{50} values were determined by sigmoidal curve fitting using Excel-based software.

5.1.5. Immunofluorescence staining of cellular microtubules

For MT staining A549 cells were cultured in 12-well plates on small glass coverslips (11 mm diameter) at a density of 2×10^4 cells per coverslip. Cells were incubated with selected compounds or nocodazole as a positive control at concentrations of 0.025, 5, and 25 μM at 37 °C and 5% CO_2 for 8 h 0.6% DMSO served as a negative control. The whole process of cell fixation and staining was described previously [39]. Fixed cells were labelled with mouse monoclonal antibody against alpha tubulin at a dilution of 1:400 (Sigma, St. Louis. USA), followed by incubation of Alexa Flour488 labelled goat anti-mouse IgG at a dilution of 1:200 (Molecular Probes, Eugene, USA). Images of all samples were acquired with a Nikon Diaphot 300 inverted microscope (Nikon GmbH, Düsseldorf, Germany) equipped with a cooled charge-couple device camera system (SenSys; Photometrics, Munich, Germany).

5.1.6. Tubulin polymerization assay

Purified tubulin was isolated from bovine brain in BRB80 buffer (80mM PIPES, pH 6.8, 1 mM MgCl₂, 1 mM EGTA) [40]. Polymerization was initialized by adding of 10% DMSO and GTP (0.5 mM) to 1.2 mg/mL tubulin solution. Tubulin samples were incubated for 1 h at 37 °C with test compounds and with nocodazole as a positive control at concentration of 10 μM, and 0.6% DMSO as a negative control. The MT assembly was analysed using VEC-DIC microscopy using a Nikon Diaphot 300 inverted microscope (Nikon GmbH, Düsseldorf, Germany) equipped with aHamamatsu C2400-07 Newvicon and ARGUS 20 image processor (Hamamatsu Photonics Deutschland GmbH, Herrsching, Germany) [41].

5.2. Computational studies

Known tubulin inhibitors were used as a reference set (Fig. S1). Smiles codes and 3D structures were gathered from PubChem database and the respective co-crystal structures with tubulin from PDB: taxol™ (1JFF), DAMA-colchicine (1SA0), podophyllotoxin (1SA1). Other compounds from this report (including CA-2 and CA-4) were modeled in Sybyl 8.1 (Tripos, Saint Louis, MO). Omega, ROCS, FRED and VIDA software were acquired from OpenEye Scientific Software Inc. (Santa Fe, NM). Omega software (v. 2.2.1) was chosen to sample the 3D conformations for all molecules using RMS = 0.3; energy window (ewindow) = 15 Kcal mol⁻¹; maximum number of conformations to be saved (maxconfs) = 1000; maximum number of conformations generated (maxconfgen) = 100,000; (fixrms) = 0.1; maximum amount of time (maxtime) = 360 s; other parameters were set as default. The coordinates of the original X-ray structures of podophyllotoxin and DAMA-colchicine were modified in order to include these conformations.

3D similarity testing was performed by Rapid Overlay of Chemical Structures (ROCS v. 2.3.1) with the default parameters and 10 chosen conformations (maxconfs). Fast Rigid Exhaustive Docking (FRED v. 2.2.3) [37] was the chosen docking program and all calculations were based on the default parameters, number of poses (num poses) = 200 and number of alternative poses (num_alt_poses) = 19. A higher than usual number of poses was selected in order to try to cover different poses and interactions between the compound and the protein, which may be captured in one of the 20 poses saved at the end of the docking procedure. The X-ray crystallographic structures of tubulin with DAMA-colchicine (1SA0) were chosen to be the reference for docking. Podophyllotoxin (1SA1 X-rays structure) was used as a reference to check the pose of this compound. Taxol does not interact with tubulin in the pocket formed at the interface of α/β subunits like colchicine and podophyllotoxin [42]. The X-ray structures of taxol (1JFF) and podophyllotoxin (1SA1) were superimposed to 1SA0 to see the partial occlusion of the colchicine binding site by the α-helix of tubulin (Fig. S3).

Two cages were built to dock the reference compounds into the 1SA0 structure (Fig. S4 and Table S1): 1). The entire interface was considered when building the lager cage, but the docking results did not support the idea that some compounds displace GTP from its binding site (not shown), so that it was not further considered in the study; 2) a smaller cage centered on the colchicine binding site provided the best results. The addition of two-point pharmacophores further improved the overall results for the dataset in study analysed in VIDA (v. 3.0.0). Two hydrophobic pharmacophores used to guide docking experiments were chosen from the set presented

in [30] Both their positioning as well as the results for a training set are displayed in Fig. S5.

Acknowledgments

Supplementary data

Supplementary data associated with this article can be found in the online version, at doi:10.1016/j.ejmech.2009.12.072.

References

[1] D. Bray, Cell Movements: From Molecules to Motility, second ed. Garland Publishing, New York, 2001.

[2] M.A. Jordan, L. Wilson, Microtubules as a target for anticancer drugs. Nat. Rev. Cancer 4 (2004) 253–265.

[3] A.S. Kiselyov, K. Balakin, S.E. Tkachenko, A.V. Ivachtchenko, Recent developments in discovery and development of antimitotic agents. Anti-Cancer Agents Med. Chem. 7 (2007) 189–208.

[4] L. Wordeman, T.J. Mitchison, Dynamics of microtubule assembly in vivo. in: J.S. Hyams, C.W. Lloyd (Eds.), Microtubules. Wiley-Liss Inc., New York, 1994, pp. 287–301.

[5] E. Hamel, Antimitotic natural products and their interactions with tubulin. Med. Res. Rev. 16 (1996) 207–231.

[6] A. Jordan, J.A. Hadfield, N.J. Laurence, A.T. McGown, Tubulin as a target for anticancer drugs: agents which interact with the mitotic spindle. Med. Res. Rev. 18 (1998) 259–296.

[7] D.G.I. Kingston, Tubulin-interactive natural products as anticancer agents. J. Nat. Prod. (2009) Jan 6 [Epub ahead of print].

[8] L. Wilson, D. Panda, M.A. Jordan, Modulation of microtubule dynamics by drugs: a paradigm for the actions of cellular regulators. Cell Struct. Funct. 24 (1999) 329–335.

[9] E. Nogales, M. Whittaker, R.A. Milligan, K.H. Downing, High-resolution model of the microtubule. Cell 96 (1999) 79–88.

[10] J.F. Diaz, R. Strobe, Y. Engelborghs, A.A. Souto, J.M. Andreu, Molecular recognition of Taxol by microtubules. Kinetics and thermodynamics of binding of fluorescent Taxol derivatives to an exposed site. J. Biol. Chem. 275 (2000) 26265–26276.

[11] R.B.G. Ravelli, B. Gigant, P.A. Curmi, I. Jourdain, S. Lachkar, A. Sobel, M. Knossow, Insight into tubulin regulation from a complex with colchicine and a stathmin-like domain. Nature 428 (2004) 198–202.

[12] E.K. Rowinsky, V. Chaudhry, D.R. Cornblath, R.C. Donehower, Neurotoxicity of taxol. J. Natl. Cancer Inst. 15 (1993) 107–115.

[13] S.P. Cole, K.E. Sparks, K. Fraser, D.W. Loe, C.E. Grant, G.M. Wilson, R.G. Deeley, Pharmacological characterization of multidrug resistant MRP-transfected human tumor cells. Cancer Res. 54 (1994) 5902–5910.

[14] A. Lorico, G. Rappa, R.A. Flavell, A.C. Sartorelli, Double knockout of the mrp gene leads to increased drug sensitivity in vitro. Cancer Res. 56 (1996) 5351–5355.

[15] P. Giannakakou, D.L. Sackett, Y.K. Kang, Z. Zhan, J.T. Buters, T. Fojo, M.S. Poruchynsky, Paclitaxel-resistant human ovarian cancer cells have mutant beta-tubulin that exhibit impaired paclitaxel-driven polymerization. J. Biol. Chem. 272 (1997) 17118–17125.

[16] M. Kavallaris, D.Y.S. Kuo, C.A. Burkhart, D.L. Regl, M.D. Norris, M. Haber, S.B. Horwitz, Taxol-resistant epithelial ovarian tumors are associated with altered expression of specific beta-tubulin isotypes. J. Clin. Invest. 100 (1997) 1282–1293.

[17] H.C. Pitot, E.A. McElroy Jr., J.M. Reid, A.J. Windebank, J.A. Sloan, C. Erlichman, P.G. Bagniewski, D.L. Walker, J. Rubin, R.M. Goldberg, A.A. Adjei, M.M. Ames, Phase I trial of Dolastatin-10 (NSC 376128) in patients with advanced solid tumors. Clin. Cancer Res. 5 (1999) 525–531.

[18] N.-H. Nam, Combretastatin A-4 analogues as antimitotic antitumor agents. Curr. Med. Chem. 10 (2003) 1697–1722.

[19] G.C. Tron, T. Pirali, G. Sorba, F. Pagliai, S. Busacca, A.A. Genazzani, Medicinal chemistry of combretastatin A-4: present and future directions. J. Med. Chem. 49 (2006) 3033–3044.

[20] S. Desbene, S. Giorgi-Renault, Drugs that inhibit tubulin polymerization: the particular case of podophyllotoxin and analogues. Curr. Med. Chem. – Anti-Cancer Agents 2 (2002) 71–90.

[21] X. Ouyang, E.L. Piatnitski, V. Pattaropong, X. Chen, H.-Y. He, A.S. Kiselyov, A. Velankar, J. Kawakami, M. Labelle, L. Smith II, J. Lohman, S.P. Lee, A. Malikzay, J. Fleming, J. Gerlak, Y. Wang, R.L. Rosler, K. Zhou, S. Mitelman, M. Camara, D. Surguladze, J.F. Doody, M.C. Tuma, Oxadiazole derivatives as a novel class of antimitotic agents: synthesis, inhibition of tubulin polymerization, and activity in tumor cell lines. Bioorg. Med. Chem. Lett. 16 (2006) 1191–1196.

[22] M. Semenova, A.S. Kiselyov, V.V. Semenov, Sea urchin embryo as a model organism for the rapid functional screening of tubulin modulators. BioTechniques 40 (2006) 765–774 video illustrations are available at. http://www.chemblock.com.

[23] M.N. Semenova, A.S. Kiselyov, I.Y. Titov, M.M. Raihstat, M. Molodtsov, E. Grishchuk, I. Spiridonov, V.V. Semenov, In Vivo evaluation of indolyl glyoxamides in the sea urchin embryo model: correlation with in vitro tubulin dynamics effects. Chem. Biol. Drug Design 70 (2007) 485–490.

[24] G.R. Pettit, S.B. Singh, M.R. Boyd, E. Hamel, R.K. Pettit, J.M. Schmidt, F. Hogan, Antineoplastic agents. 291. Isolation and synthesis of combretastatins A-4, A-5, and A-6. J. Med. Chem. 38 (1995) 1666–1672.

[25] X. Ouyang, A. Kiselyov, X. Chen, H.-Y. He, J. Kawakami, V. Pattaropong, E. Piatnitski, M.C. Tuma, J. Kincaid, Heterocyclic compounds and their use as anticancer agents, Patent WO 2005/004818 A2, (2005).

[26] T. Mosmann, Rapid colorimetric assay for cellular growth and survival: application to proliferation and cytotoxicity assays. J. Immunol. Methods 65 (1983) 55–63.

[27] P.C.D. Hawkins, A.G. Skillman, A. Nicholls, Comparison of shape-matching and docking as virtual screening tools. J. Med. Chem. 50 (2007) 74–82.

[28] C.M. Lin, S.B. Singh, P.S. Chu, R.O. Dempcy, J.M. Schmidt, G.R. Pettit, E. Hamel, Interactions of tubulin with potent natural and synthetic analogs of the antimitotic agent combretastatin: a structure-activity study. Mol. Pharmacol. 34 (1988) 200–208.

[29] G. Bacher, B. Nickel, P. Emig, U. Vanhoefer, S. Seeber, A. Shandra, T. Klenner, T. Beckers, D-24851, a novel synthetic microtubule inhibitor, exerts curative antitumoral activity in vivo, shows efficacy toward multidrug-resistant tumor cells, and lacks neurotoxicity. Cancer Res. 61 (2001) 392–399.

[30] A. Couture, E. Deniau, P. Grandclaudon, S. Lebrun, S. Léonce, P. Renard, B. Pfeiffer, First synthesis and pharmacological evaluation of benzoindolizidine and benzoquinolizidine analogues of α- and β-peltatin. Bioorg. Med. Chem. 8 (2000) 2113–2125.

[31] http://eyesopen.com/products/applications/omega.html.

[32] http://eyesopen.com/products/applications/rocs.html.

[33] S. Fortin, E. Moreau, J. Lacroix, J.-C. Teulade, A. Patenaudea, R. Gaudreaulta, N-Phenyl- N'-(2-chloroethyl)urea analogues of combretastatin A-4: is the N-phenyl-N'-(2-chloroethyl)urea pharmacophore mimicking the trimethoxy phenyl moiety. Bioorg. Med. Chem. Lett. 17 (2007) 2000–2004.

[34] T.L. Nguyen, C. McGrath, A.R. Hermone, J.C. Burnett, D.W. Zaharevitz, B.W. Day, P. Wipf, E. Hamel, R. Gussio, A common pharmacophore for a diverse set of colchicine site inhibitors using a structure-based approach. J. Med. Chem. 48 (2005) 6107–6116.

[35] A. Chaudhary, S.N. Pandeya, P. Kumar, P.P. Sharma, S. Gupta, N. Soni, K.K. Verma, G. Bhardwaj, Combretastatin A-4 analogs as anticancer agents. Mini Rev. Med. Chem. 7 (2007) 1186–1205.

[36] X. Ouyang, X. Chen, E.L. Piatnitskii, A.S. Kiselyov, H.-Y. He, Y. Mao, V. Pattaropong, Y. Yu, K.H. Kim, J. Kincaid, L. Smith II, W.C. Wong, S.P. Lee, D.L. Milligan, A. Malikzay, J. Fleming, J. Gerlak, D. Dhanvanthri, J.F. Doody, H.-H. Chiang, S.N. Patel, Y. Wang, R.L. Rosler, P. Kussie, M. Labelle, M.C. Tuma, Synthesis and structure-activity relationships of 1,2,4-triazoles as a novel class of tubulin polymerization inhibitors. Bioorg. Med. Chem. Lett. 15 (2005) 5154–5159.

[37] M.R. McGann, H.R. Almond, A. Nicholls, J.A. Grant, F.K. Brown, Gaussian docking functions. Biopolymers 68 (2003) 76–90.

[38] K. Gewald, P. Belimann, Syntese und reactionen von 4-aminoisothiazolen. Liebigs Ann. Chem. (1979) 1534–1546.

[39] A. Al-Haddad, M.A. Shonn, B. Redlich, A. Blocker, J.K. Burkhardt, H. Yu, J.A. Hammer 3rd, D.G. Weiss, W. Steffen, G. Griffiths, S.A. Kuznetsov, Myosin Va bound to phagosomes binds to F-actin and delays microtubule-dependent motility. Mol. Biol. Cell. 12 (2001) 2742–2755.

[40] S.A. Kuznetsov, V.I. Rodionov, A.D. Bershadsky, V.I. Gelfand, V.A. Rosenblat, High molecular weight protein MAP2 promoting microtubule assembly in vitro is associated with microtubules in cells. Cell Biol. Int. Rep. 4 (1980) 1017–1024.

[41] D.G. Weiss, W. Maile, R.A. Wick, W. Steffen, Video microscopy. in: A.J. Lacey (Ed.), Light Microscopy in Biology. A Practical Approach, second ed. Oxford University Press, USA, 1999, pp. 73–105.

[42] J. Löwe, H. Li, K.H. Downing, E. Nogales, Refined structure of áâ-tubulin at 3.5 Å. J. Mol. Biol. 313 (2001) 1045–1057.